Chinese Chemical Letters 34 (2023) 107688

Contents lists available at ScienceDirect

Chinese Chemical Letters

journal homepage: www.elsevier.com/locate/cclet

Highly emissive perylene diimide-based bowtie-shaped metallacycles

Yali Hou[1], Ruping Shi[1], Hongye Yuan*, Mingming Zhang*

State Key Laboratory for Mechanical Behavior of Materials, Shaanxi International Research Center for Soft Matter, School of Materials Science and Engineering, Xi'an Jiaotong University, Xi'an 710049, China

ARTICLE INFO

Article history:
Received 7 May 2022
Revised 9 July 2022
Accepted 15 July 2022
Available online 19 July 2022

Keywords:
Fluorescence materials
Emissive metallacycles
Self-assembly
Perylene diimide
Picric acid sensing

ABSTRACT

Metallacycles hold great promise for fluorescence-based sensing due to their synthetic advantages and unique physicochemical properties. However, it remains highly challenging to develop a versatile methodology for constructing highly emissive metallacycles with targeted functionalities and therefore sought-after properties. Herein, we report a general strategy to construct a series of highly emissive perylene diimide-based metallacycles *via* the self-assembly of perylene diimide-based tetrapyridyl ligand with different dicarboxylic ligands featuring fixed angles and *cis*-$Pt(PEt_3)_2(OTf)_2$. Single crystal X-ray diffraction analyses verify the formation of bowtie-like metallacycles with two triangular cavities. Notably, the fluorescence quantum yields of most assemblies exceed 98%, amongst the highest values for metallacycles. Additionally, such metallacycles exhibit sensitive fluorescence responses toward picric acid with a detection limit of 2.8×10^{-6} mol/L. This study not only provides a rational strategy for preparing highly emissive bowtie-shaped metallacycles, but also sheds light on their usage in the detection of picric acid and associated compounds.

Fluorescent materials have been extensively studied over the past decades because of their wide applications in bioimaging [1,2], chemosensing [3,4], optoelectronics [5,6], *etc.* In particular, fluorescence-based sensors have become one of the leading sensing technologies due to their fast response, easy visualization, and high sensitivity and selectivity [7,8]. As a result, the development of novel fluorescence-based sensors has received ever-growing interests. Conventional small molecule fluorophores, conjugated organic/inorganic polymers and dendrimers have been widely developed so far with a special emphasis on fluorescent sensing purposes [9,10]. Specifically, conjugated polymers (CPs) are composed of backbones possessing π-conjugated subunits, and thus benefit from electron delocalization. This endows CPs high sensitivity and selectivity toward fluorescent sensing [11–13]. Nevertheless, the preparation of CPs typically involves several synthetic steps and exhibits relatively inferior molecular organization, which greatly impedes their multitudinous applications. Substantial efforts have been made in addressing such issues, within which the coordination-driven self-assembly method outstands. Unlike the stepwise covalent synthetic protocols, this strategy is facile yet highly efficient due to its synthetic advantages, including high degree of predictability, inherent self-correction, fewer steps and traceability [14–19].

Metallacycles, as an important type of metallosupramolecules, are constructed by coordination-driven self-assembly, and their topology and physicochemical properties can be finely tuned by judicious choices of building units with variable numbers, locations, relative orientations, and additional functional moieties [20–27]. For instance, perylene diimide (PDI) derivatives [28–34], as archetypal fluorophores with excellent optical and electrochemical properties, have been utilized as large rigid and planar scaffolds to construct luminescent metallacycles and metallacages. Such assemblies not only inherit the photophysical properties of their building fluorophore moieties but also exhibit novel features that are not observable for the single components, such as tunable emission wavelengths, markedly enhanced fluorescence efficiencies, and selective response toward specific molecules. Although significant progress has been made on the design and synthesis of emissive metallacycles, a universal strategy for constructing novel emissive metallacycles is highly desirable but remains absent.

Herein, we develop a strategy to build a series of metallacycles **4a–4f** by multicomponent coordination-driven self-assembly. Notably, the methodology relies mainly on the stoichiometry of the individual building units, as well as the geometry and length of the ligands. As shown in Scheme 1, these metallacycles include three parts: PDI-based tetrapyridyl ligand (**1**), dicarboxylic ligands (**2a–2f**) and *cis*-$Pt(PEt_3)_2(OTf)_2$ (**3**). Interestingly, these met-

* Corresponding authors.
E-mail addresses: hongye.yuan@xjtu.edu.cn (H. Yuan), mingming.zhang@xjtu.edu.cn (M. Zhang).
[1] These authors contributed equally to this work.

https://doi.org/10.1016/j.cclet.2022.07.031
1001-8417/

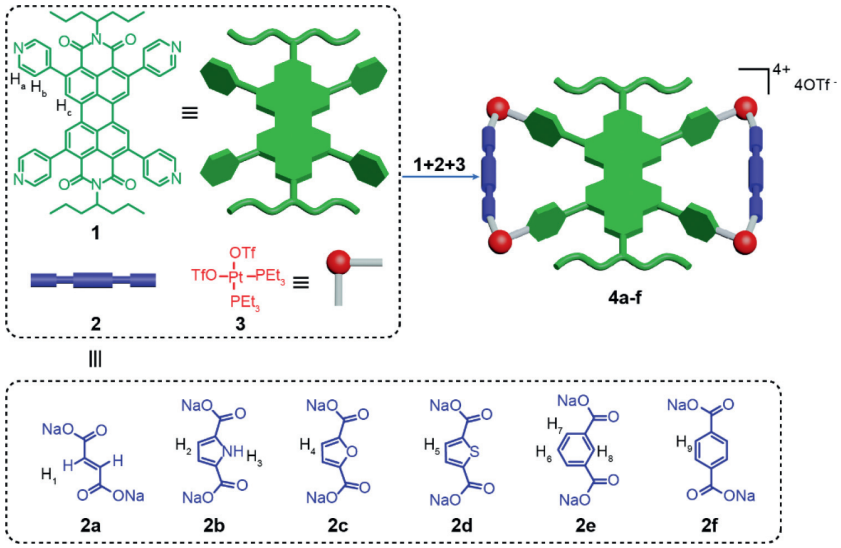

Scheme 1. Cartoon representations of the self-assembly of bowtie-shaped metallacycles **4a**–**4f**.

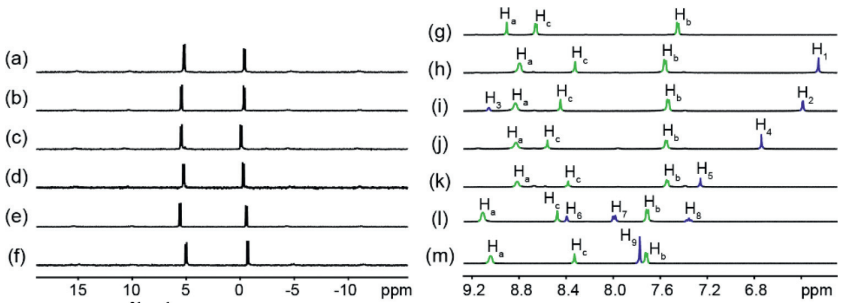

Fig. 1. Partial $^{31}P\{^1H\}$ NMR spectra (121.4 MHz, CD_3CN, 295 K) of **4a** (a), **4b** (b), **4c** (c), **4d** (d), **4e** (e) and **4f** (f). Partial ^1H NMR spectra (400 MHz, CD_3CN, 295 K) of **1** (g), **4a** (h), **4b** (i), **4c** (j), **4d** (k), **4e** (l) and **4f** (m).

allacycles show symmetrical, bowtie-like shapes in solid-state and bright emission in acetonitrile with fluorescence quantum yields (Φ_F) exceeding 98% for metallacycles **4a**, **4c–4f**. Moreover, these metallacycles display fluorescence decays in response to variable concentrations of picric acid (PA) with a low detection limit of 2.8×10^{-6} mol/L (S/N = 3), comparable to the reported values from literature. This study describes a versatile strategy for the design and preparation of highly emissive bowtie-shaped metallacycles as fluorescence-based sensors, which will certainly promote the development of metallacycles for chemosensing applications.

The formation of bowtie-shaped metallacycles **4a–4f** was confirmed by multiple techniques including $^{31}P\{^1H\}$, ^1H NMR and electrospray ionization time-of-flight mass spectrometry (ESI-TOF-MS). As shown in Figs. 1a–f, the $^{31}P\{^1H\}$ NMR spectra of **4a–4f** split into two doublet peaks at 5.13 ppm and −0.47 ppm for **4a**, 5.38 ppm and −0.42 ppm for **4b**, 5.40 ppm and −0.14 ppm for **4c**, 5.18 ppm and −0.35 ppm for **4d**, 4.95 ppm and −0.76 ppm for **4e**, and 5.51 ppm and −0.64 ppm for **4f**, respectively. These two doublet peaks nearly share equal intensities with concomitant ^{195}Pt satellites, corresponding to different phosphorus environments. This result clearly indicates the formation of discrete symmetric metallacycles. The α-pyridyl protons H_a and β-pyridyl protons H_b (Figs. 1g–m) of ligand **1** in metallacycles **4a–f** were noticed, showing obvious downfield chemical shifts compared to free ligand **1**. Investigation of the ESI-TOF-MS provides further support for the stoichiometry of **4a–4f** (Figs. S32, S36, S40, S44, S48, S52 in Supporting information). Accordingly, the observed peaks are consistent with the calculated ones. For instance, peaks at *m/z* 998.8642, 1024.8661, 1025.5089, 1036.1442, 1032.2203 and 1032.2203 were found, corresponding to $[\mathbf{4a}\text{–}3OTf]^{3+}$, $[\mathbf{4b}\text{–}3OTf]^{3+}$, $[\mathbf{4c}\text{–}3OTf]^{3+}$, $[\mathbf{4d}\text{–}3OTf]^{3+}$, $[\mathbf{4e}\text{–}3OTf]^{3+}$ and $[\mathbf{4f}\text{–}3OTf]^{3+}$, respectively. All these results evidenced the successful formation of the bowtie-shaped metallacycles **4a–4f**.

Dark red single crystals **4a–4f** suitable for X-ray diffraction analysis were successfully obtained by slow evaporation of dioxane into the DMF solution (vapors of dioxane are diffusing into DMF) of metallacycles. The crystal structures of metallacycles **4a–4f** are shown in Figs. 2a–f, which unambiguously confirms their two-dimensional bowtie-shaped structures. X-ray crystallographic analyses suggest that these metallacycles share similar structures in which the pyridyl groups and carboxylic groups are linked by four platinum atoms, leading to the formation of a [1 + 2 + 4] structure. Based on the distances between the platinum atoms, the length and width of metallacycles **4a–4f** are 1.68×0.97 nm, 1.66×1.07 nm, 1.64×1.06 nm, and 1.64×1.06 nm, 1.67×1.07 nm and 1.63×1.11 nm (Figs. 2a–f), respectively. Metallacycles **4a–4c**, **4e** and **4f** exhibit the same packing mode (Fig. S1 in Supporting information), with the metallacycle units aligned linearly *via* intermolecular interactions. Dissimilarly, the **4d** metallacycles reassemble into parallelepipeds, where two adjacent metallacycles are connected by two C–H···O interactions ($d_{H\cdots O\ plane} = 2.61$ Å) between PDI and $CF_3SO_3^-$ anions and four F···π interactions ($d_{F\cdots\pi\ plane} = 3.11$–$3.14$ Å) between $CF_3SO_3^-$ anions and PDI. Moreover, the neighboring metallacycle **4d** belonging to different parallel pipelines is connected by C–H···O ($d_{H\cdots O\ plane} = 2.39$–$2.62$ Å). This observation is in accordance with that of previous studies

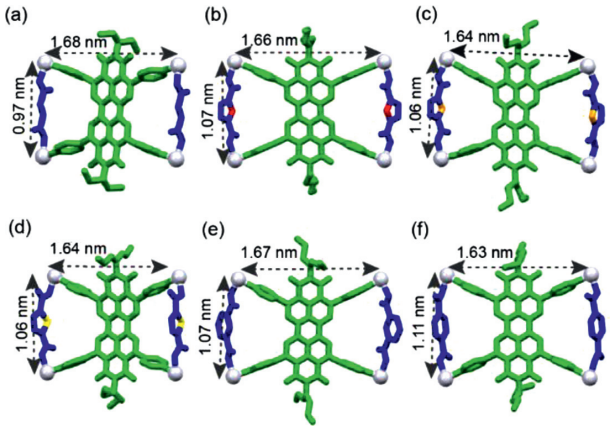

Fig. 2. Crystal structures of **4a** (a), **4b** (b), **4c** (c), **4d** (d), **4e** (e) and **4f** (f). Hydrogen atoms, counterions, solvent molecules and triethylphosphine units are omitted for clarity.

Table 1
UV-vis absorption and fluorescence emission data.[a]

Sample	Absorption bands (nm)			Emission bands (nm)		Φ_F [b] (%)
1	456	487	522	540	578	95
4a	456	487	522	539	577	99
4b	456	487	522	541	579	32
4c	456	487	522	541	579	99
4d	456	487	522	541	579	98
4e	456	487	522	541	579	99
4f	456	487	522	541	579	99

[a] Measurements were performed in CH_3CN unless otherwise noted. The excitation wavelength is 365 nm for **1** and **4a–4f**.
[b] Fluorescence quantum yield.

[35,36]. In such a manner, the packing mode in **4d** was finally formed and different from other metallacycles, which may be rationalized by their different growth environments.

The UV-vis absorption and fluorescence emission spectra of ligand **1** and metallacycles **4a–4f** are depicted Table 1, Fig. S52 and Table S3 (Supporting information). The UV-vis absorption spectra for both ligand **1** and metallacycles **4a–4f** exhibit three absorption bands centered at 456 nm, 487 nm, and 522 nm, respectively. Metallacycles **4a–4f** display absorption bands similar to those of ligand **1** because of the weak absorption of carboxylic ligands **2a–2f** compared with PDI. Similarly, the fluorescence emission of all the metallacycles exhibit similar curves, with an intense peak centered at 540 nm. Noticeably, the fluorescence intensities of metallacycles **4a**, **4c**–**4f** are all higher than that of ligand **1**, whereas the intensity of metallacycle **4b** is much lower than that of ligand **1** under identical conditions**.** The fluorescence quantum yields of metallacycles **4a**, **4c**–**4f** in CH_3CN reached 99%, 99%, 98%, 99% and 99% (Table 1 and Figs. S2–S9 in Supporting information), respectively. However, owing to the introduction of an electron-donating group (-NH-) into metallacycle **4b**, its Φ_F value is only 32%, because the photoinduced electron transfer (PET) from the NH groups to the fluorophore offers a non-radiative pathway to quench the emission [37].

Nitroaromatic compounds are widely used in firework manufacturing, chemical industry, leather, pharmaceutical, and dye industries. Leakage of nitroaromatic compounds during production and transportation not only pollutes the groundwater and soil environments, but also poses great threats to human beings. Therefore, the rapid detection of these compounds has always been an important task [38].

To explore the potential application of the metallacycles in the detection of nitroaromatic compounds, we chose picric acid as a model compound to perform fluorescence titration tests. As shown

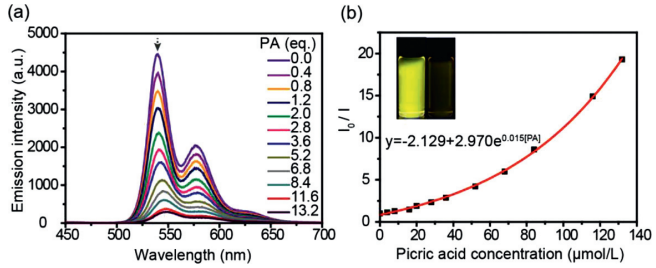

Fig. 3. Fluorescence spectra of **4a** (a) with increased amounts of picric acid ($c = 10$ μmol/L in metallacycle concentration, $\lambda_{ex} = 365$ nm). Stern-Volmer plot I_0/I *versus* the concentration of picric acid (b). The inset denotes the fluorescent photographs before and after the addition of picric acid.

in Fig. 3a, with the addition of picric acid, the emission intensity of metallacycle **4a** gradually decreased. Once the addition of picric acid reached a ratio of 13 equiv., its emission was almost completely quenched. Correspondingly, the quenching constant was determined to be 5.2×10^4 L/mol by nonlinear fitting (Fig. 3b), and the detection limit was 2.8×10^{-6} mol/L (S/N = 3), comparable with the reported values from literature [39–42]. This quenching process can be directly noticed by naked eyes. Similar quenching phenomena were also observed for other bowtie-shaped metallacycles **4b–4f** (Figs. S53–S57 and Table S4 in Supporting information), indicating their potential use as chemical sensors for the detection of nitroaromatic compounds.

In summary, a series of PDI-based bowtie-shaped metallacycles were successfully constructed by coordination-driven multicomponent self-assembly. Their structures were well resolved by single crystal X-ray diffraction analysis. Moreover, most metallacycles showed remarkable fluorescence quantum yields in CH_3CN and all metallacycles experienced fluorescence quenching upon the addition of variable concentrations of picric acid. The detection limit can reach as low as 2.8×10^{-6} mol/L. These findings clearly indicate that such metallacycles can be used as fluorescent sensors for the detection of nitroaromatic compounds. This work justifies our strategy to systematically prepare metallacycles with tailor-made photophysical and chemical properties, which will promote the development of functional metallacycles and their applications in various scenarios.

Declaration of competing interest

The authors declare that they have no known competing financial interests or personal relationships that could have appeared to influence the work reported in this paper.

Acknowledgments

This work was supported by the National Natural Science Foundation of China (No. 22171219), and the Fundamental Research Funds for the Central Universities (No. xzy022021004). We thank Dr. Gang Chang at the Instrument Analysis Center and Dr. Aqun Zheng and Junjie Zhang at the Experimental Chemistry Center of Xi'an Jiaotong University for NMR and fluorescence measurements.

Supplementary materials

Supplementary material associated with this article can be found, in the online version, at doi:10.1016/j.cclet.2022.07.031.

References

[1] J.T. Hou, W.X. Ren, J.S. Kim, et al., Chem. Soc. Rev. 46 (2017) 2076–2090.
[2] M. Collot, Mater. Horiz. 8 (2021) 501–514.
[3] S. Shanmugaraju, P.S. Mukherjee, Chem. Commun. 51 (2015) 16014–16032.

[4] T.L. Mako, J.M. Racicot, M. Levine, Chem. Rev. 119 (2019) 322–477.
[5] V.W. Yam, V.K. Au, S.Y. Leung, Chem. Rev. 115 (2015) 7589–7728.
[6] M.P. Duffy, W. Delaunay, P.A. Bouit, M. Hissler, Chem. Soc. Rev. 45 (2016) 5296–5310.
[7] M. Jiang, X. Gu, B.Z. Tang, et al., Chem. Sci. 8 (2017) 5440–5446.
[8] S. Cui, Y. Wu, J. Wang, et al., Chin. Chem. Lett. 31 (2020) 487–493.
[9] O.S. Wolfbeis, Chem. Soc. Rev. 44 (2015) 4743–4768.
[10] M. Gao, B.Z. Tang, ACS Sens. 2 (2017) 1382–1399.
[11] T. Repenko, A. Rix, A.J.C. Kuehne, et al., Nat. Commun. 8 (2017) 470.
[12] W. Wu, G.C. Bazan, B. Liu, Nat. Chem. 2 (2017) 760–790.
[13] T.F. Abelha, C.A. Dreiss, M.A. Green, L.A. Dailey, J. Mater. Chem. B 8 (2020) 592–606.
[14] K. Harris, D. Fujita, M. Fujita, Chem. Commun. 49 (2013) 6703–6712.
[15] L. Xu, Y.X. Wang, L.J. Chen, H.B. Yang, Chem. Soc. Rev. 44 (2015) 2148–2167.
[16] T.R. Cook, P.J. Stang, Chem. Rev. 115 (2015) 7001–7045.
[17] G.H. Clever, P. Punt, Acc. Chem. Res. 50 (2017) 2233–2243.
[18] M. Pan, K. Wu, J.H. Zhang, C.Y. Su, Coord. Chem. Rev. 378 (2019) 333–349.
[19] S. Tashiro, M. Shionoya, Acc. Chem. Res. 53 (2020) 632–643.
[20] Y.X. Hu, X. Zhang, L. Xu, H.B. Yang, Isr. J. Chem. 59 (2018) 184–196.
[21] G.Y. Wu, L.J. Chen, H.B. Yang, et al., Coord. Chem. Rev. 369 (2018) 39–75.
[22] L. Ma, T. Yang, M. Zhang, et al., Chin. Chem. Lett. 30 (2019) 1942–1946.
[23] Y. Sun, C. Chen, J. Liu, P.J. Stang, Chem. Soc. Rev. 49 (2020) 3889–3919.
[24] E.G. Percástegui, V. Jancik, Coord. Chem. Rev. 407 (2020) 213165.
[25] Z. Guo, J. Zhao, X. Yan, et al., Chin. Chem. Lett. 32 (2021) 1691–1695.
[26] H. Liu, Z. Zhang, M. Zhang, et al., Angew. Chem. Int. Ed. 61 (2022) e202207289.
[27] Z. Zhang, L. Ma, M. Zhang, et al., JACS Au 2 (2022) 1479–1487.
[28] S. Chen, P. Slattum, C. Wang, L. Zang, Chem. Rev. 115 (2015) 11967–11998.
[29] P.D. Frischmann, V. Kunz, F. Wurthner, Angew. Chem. Int. Ed. 54 (2015) 7285–7289.
[30] F. Wurthner, C.R. Saha-Moller, D. Schmidt, et al., Chem. Rev. 116 (2016) 962–1052.
[31] Y. Hou, Z. Zhang, M. Zhang, et al., J. Am. Chem. Soc. 142 (2020) 18763–18768.
[32] Q.H. Ling, J.L. Zhu, Y. Qin, L. Xu, Mater. Chem. Front. 4 (2020) 3176–3189.
[33] X. Chang, S. Lin, P.J. Stang, et al., J. Am. Chem. Soc. 142 (2020) 15950–15960.
[34] Y. Hou, Z. Zhang, M. Zhang, et al., CCS Chem. 3 (2021) 3153–3160.
[35] Z. Yang, Y. Wang, P.J. Stang, et al., J. Am. Chem. Soc. 142 (2020) 13689–13694.
[36] H. Duan, Y. Li, L. Cao, et al., Angew. Chem. Int. Ed. 59 (2020) 10101–10110.
[37] J.L. Zhu, L. Xu, H.B. Yang, et al., Nat. Commun. 10 (2019) 4285.
[38] K.S. Ju, R.E. Parales, Microbiol. Mol. Biol. Rev. 74 (2010) 250–272.
[39] Y. Hu, M. Ding, X.Q. Liu, L.B. Sun, H.L. Jiang, Chem. Commun. 52 (2016) 5734–5737.
[40] L. Zhang, Y. Sun, Z. Yao, et al., Chin. Chem. Lett. 31 (2020) 2428–2432.
[41] Y. Hou, S. Li, Z. Zhang, L. Chen, M. Zhang, Polym. Chem. 11 (2020) 254–258.
[42] Z.Y. Li, Z.Q. Yao, X.H. Bu, et al., Chin. Chem. Lett. 32 (2021) 3095–3098.